A Comparison of Model- and Satellite-Derived Aerosol Optical Depth and Reflectivity

JOYCE E. PENNER,[a] SOPHIA Y. ZHANG,[a] MIAN CHIN,[b] CATHERINE C. CHUANG,[c] JOHANN FEICHTER,[d] YAN FENG,[a] IGOR V. GEOGDZHAYEV,[e] PAUL GINOUX,[b] MICHAEL HERZOG,[a] AKIKO HIGURASHI,[f] DOROTHY KOCH,[e] CHRISTINE LAND,[d] ULRIKE LOHMANN,[g] MICHAEL MISHCHENKO,[e] TERUYUKI NAKAJIMA,[h] GIOVANNI PITARI,[i] BRIAN SODEN,[j] INA TEGEN,[k] AND LAWRENCE STOWE[l]

[a]*Department of Atmospheric, Oceanic, and Space Sciences, University of Michigan, Ann Arbor, Michigan*
[b]*Goddard Space Flight Center, Greenbelt, Maryland*
[c]*Atmospheric Sciences Division, Lawrence Livermore National Laboratory, Livermore, California*
[d]*Max Planck Institute for Meteorology, Hamburg, Germany*
[e]*Goddard Institute for Space Studies, New York, New York*
[f]*National Institute of Environmental Studies, Ibaraki, Japan*
[g]*Dalhousie University, Halifax, Nova Scotia, Canada*
[h]*Center for Climate System Research, The University of Tokyo, Tokyo, Japan*
[i]*Dipartimento di Fisica, Università de L'Aquila, L'Aquila, Italy*
[j]*Geophysical Fluid Dynamics Laboratory, Princeton University, Princeton, New Jersey*
[k]*Max Planck Institute for Biogeochemistry, Jena, Germany*
[l]*NOAA/NESDIS, Office of Research and Applications, Satellite Research Laboratory, Washington, D.C.*

(Manuscript received 22 December 2000, in final form 30 July 2001)

ABSTRACT

The determination of an accurate quantitative understanding of the role of tropospheric aerosols in the earth's radiation budget is extremely important because forcing by anthropogenic aerosols presently represents one of the most uncertain aspects of climate models. Here the authors present a systematic comparison of three different analyses of satellite-retrieved aerosol optical depth based on the Advanced Very High Resolution Radiometer (AVHRR)-measured radiances with optical depths derived from six different models. Also compared are the model-derived clear-sky reflected shortwave radiation with satellite-measured reflectivities derived from the Earth Radiation Budget Experiment (ERBE) satellite.

The three different satellite-derived optical depths differ by between −0.10 and 0.07 optical depth units in comparison to the average of the three analyses depending on latitude and month, but the general features of the retrievals are similar. The models differ by between −0.09 and +0.16 optical depth units from the average of the models. Differences between the average of the models and the average of the satellite analyses range over −0.11 to +0.05 optical depth units. These differences are significant since the annual average clear-sky radiative forcing associated with the difference between the average of the models and the average of the satellite analyses ranges between −3.9 and 0.7 W m^{-2} depending on latitude and is −1.7 W m^{-2} on a global average annual basis. Variations in the source strengths of dimethylsulfide-derived aerosols and sea salt aerosols can explain differences between the models, and between the models and satellite retrievals of up to 0.2 optical depth units.

The comparison of model-generated reflected shortwave radiation and ERBE-measured shortwave radiation is similar in character as a function of latitude to the analysis of modeled and satellite-retrieved optical depths, but the differences between the modeled clear-sky reflected flux and the ERBE clear-sky reflected flux is generally larger than that inferred from the difference between the models and the AVHRR optical depths, especially at high latitudes. The difference between the mean of the models and the ERBE-analyzed clear-sky flux is 1.6 W m^{-2}.

The overall comparison indicates that the model-generated aerosol optical depth is systematically lower than that inferred from measurements between the latitudes of 10° and 30°S. It is not likely that the shortfall is due to small values of the sea salt optical depth because increases in this component would create modeled optical depths that are larger than those from satellites in the region north of 30°N and near 50°S. Instead, the source strengths for DMS and biomass aerosols in the models may be too low. Firm conclusions, however, will require better retrieval procedures for the satellites, including better cloud screening procedures, further improvement of the model's treatment of aerosol transport and removal, and a better determination of aerosol source strengths.

Corresponding author address: Joyce E. Penner, Dept. of Atmospheric, Oceanic, and Space Sciences, University of Michigan, Ann Arbor, MI 48109-2143.
E-mail: penner@umich.edu

1. Introduction

Tropospheric aerosols act to significantly alter the earth's radiation budget, but quantification of the change in radiation is difficult because atmospheric aerosol distributions vary greatly in type, size, space, and time. The (dry) optical properties are determined by the (dry) aerosol size distribution, while the change in optical properties as a function of relative humidity is determined by the composition of the aerosol and its effect on water uptake. The monthly average variations in aerosol type as a function of space and time depend primarily on the proximity of sources of the different aerosol types and whether these sources change with season and over time. Absorbing components within the aerosols affect the relative amounts of scattered and absorbed radiation.

Tropospheric aerosols have a relatively short lifetime (5–10 days) and a high degree of variability. Partly as a result of this variability, models have become the primary means used for assessing the global atmospheric effects of aerosols. Most models used for assessments have been compared with observations to some extent. The most useful observations for this purpose have mainly been observations that extend over several years in duration, and surface-based observational data have been used for most aerosol model validations. Unfortunately, some of the surface-based aerosol composition data are only available during short duration campaigns (e.g., organic and black carbon; Penner et al. 2001). Measurements of aerosol vertical distributions for comparison to models are only available on a limited basis.

Unfortunately, surface-based observations can not be used to fully validate models. The recent Intergovernmental Panel in Climate Change (IPCC)-sponsored aerosol model intercomparison, for example, found that the absolute error between modeled and observed monthly average aerosol sulfate ranged from 15% to 46%, but the column burdens for these same models differed by more than a factor of 2 (Penner et al. 2001). The variations in column burdens for other aerosol types were even larger. Since aerosol forcing is mainly related to the column burden, it is these latter differences between the models that must be reduced in order to build confidence that we can adequately model the properties needed to determine aerosol forcing.

One measure of aerosol column burden is aerosol optical depth. This measure has the disadvantage (from the standpoint of determining forcing) of not distinguishing between different aerosol types or between anthropogenic aerosols and natural aerosols. However, aerosol optical depth is now generally available from several different analysis of Advanced Very High Resolution Radiometer (AVHRR) data (Stowe et al. 1997; Mishchenko et al. 1999; Nakajima and Higurashi 1998; Higurashi et al. 2000) and is becoming available from other satellite platforms [e.g., Polarization and Directionality of the Earth's Reflectances, POLDER (Deuze et al. 1999); multiangle imaging spectroradiometer, MISER (Kahn et al. 1997); and moderate resolution imaging spectroradiometer (MODIS; Tanré et al. 1999)]. Thus, comparison of total aerosol partical optical depth from models provides one means of assessing aerosol column burden (e.g., Tegen et al. 1997). Because aerosols act to increase the amount of radiation reflected by the planet, a second method of assessing the total aerosol amount in models has been used. This method relies on the difference in the modeled and observed broadband cloud-free reflected irradiance (Haywood et al. 1999). Below, we also explore this technique.

Here, we compare aerosol optical depth from the models that participated in the IPCC Aerosol Model Intercomparison Workshop to optical depth inferred from the AVHRR satellite analysis. Also compared are reflected radiation from these models to that from Earth Radiation Budget Experiment (ERBE; Harrison et al. 1990). We examine the uncertainty in aerosol optical depth over ocean regions associated with the prediction of column burden by the different models as well as the uncertainty associated with how optical depth is evaluated from column burden. The former uncertainty is mainly related to differences in model procedures for determining transport and scavenging. While important the reasons for such differences are not highlighted here, though they are examined in other model intercomparison studies (Jacob et al. 1997; Rasch et al. 2000; Barrie et al. 2001). The latter uncertainty involves both the determination of optical properties from aerosol mass and the uncertainty associated with how relative humidity is determined in the models that we do examine. Persistent differences between all the models and the observations may be used to identify incorrect source strengths in the models or a persistent error in the treatment of aerosol transport and removal in the models.

In the following section we first describe the available retrieved data for optical depth and reflectivity from satellites. Then we briefly describe the models used in this intercomparison and the specified emissions used in the model simulations. Section 3 describes the aerosol optical properties used in the determination of optical depth. In section 4 we compare the model-derived inline optical depths as well as an offline calculation of optical depth to the satellite-retrieved optical depths from AVHRR. Section 5 compares the models with the reflected radiation inferred from the ERBE satellite. Finally section 6 presents a discussion and our conclusions.

2. Observations and models

Satellite retrievals of aerosol optical depth are difficult because they must accurately determine the contribution of clouds, the surface, and the Rayleigh scattering atmosphere to reflected radiation. In addition, the effects of water vapor and other gaseous absorption on the observed radiances within any given channel must

be considered prior to any retrieval of aerosol properties (Mishchenko et al. 1999). Even when these parameters are accurately known, the aerosol retrieval must still depend on aerosol column thickness, real and imaginary parts of the refractive index, and the effective radius of the aerosol size distribution. Normally, in spite of the variation in aerosol size expected with relative humidity, the effective radius as well as the real and imaginary parts of the refractive index are assumed, allowing a determination of aerosol optical thickness. If more than one wavelength is used in the retrieval, the effect of aerosol size on optical depth can be improved and a retrieval of Ångström coefficient is also possible (Mischenko et al. 1999).

One of the largest sources of uncertainty in retrieval of aerosol optical depth is that associated with the cloud screening algorithm. Mischenko et al. (1999) show that differences in the cloud-screening algorithms can lead to differences in optical thickness of 0.1 or larger. In retrieving optical depth, Mischenko et al. (1999) use a modified International Satellite Cloud Climatology Program (ISCCP) cloud-screening criteria that retains only pixels with IR temperatures warmer than 1°C above the values composited from 5-day IR temperatures. Unlike clouds, the expected effect of aerosols on the reflected radiation at 650 and 850 nm should exhibit a strong decrease with wavelength. Hence Mischenko et al. (1999) also required that the observed channel 1 (λ = 650 nm) to channel 2 (λ = 850 nm) radiance ratio be in the range between 1.5 and 3.5. This cloud-screening algorithm is significantly more conservative than that from the normal ISCCP cloud-screening process (which is mainly concerned with filtering out clear skies).

Another important uncertainty in retrieval of aerosol optical depths is the calibration of the AVHRR instruments. Measured AVHRR radiances are typically only known to 5%–10%. This can lead to significant uncertainties in derived optical depth. For example, use of the postlaunch calibration for National Oceanic and Atmospheric Administration Satellite *NOAA-9*, decreased derived optical depths by of order 0.1 in open-ocean regions (Mischenko et al. 1999). Thus, the use of optical depths derived with the prelaunch calibration as an absolute measure of aerosol abundance is questionable.

In this paper, we compare the model-derived optical depth to the postlaunch calibration retrievals of optical depth from Mishchenko et al. (1999) for the time period February 1985 to October 1988. We also consider the derived optical depths of Stowe et al. (1997) for the same time period as well as those of Nakajima and Higurashi (1998) and Higurashi et al. (2000) for the year 1990. To gauge the accuracy of the satellite retrievals, Fig. 1 compares the monthly average optical depths at 0.55 μm from the analysis of Mishchenko et al. (1999), Higurashi et al. (2000), and Stowe et al. (1997) to the monthly average aerosol optical depths from the ground-based Aerosol Robotic Network (AERONET) network of sunphotometers (Holben et al. 2001). The data from Mishchenko et al. (1999) and Stowe et al. (1997) are for the time period February 1985 through October 1988, while the data from Higurashi et al. (2000) are for 1990, and the time periods for the AERONET data are for the late 1990s (see figure). There are notable differences between the satellite-derived optical depth and those from AERONET at the different stations. For example, the correlation coefficients between the retrieved optical depth and AERONET data are only 0.36, 0.64, and 0.52 for the analysis of Mishchenko et al. (1999), Higurashi et al. (2000), and Stowe et al. (1997), respectively. The discrepancies may be because of the different years analyzed for each of the sensors. For example, the Mishchenko et al. (1999) and Stowe et al. (1997) satellite retrievals refer to an average of 1985 to 1988, whereas the AERONET data were collected after 1990 (see figure caption). The effect of year-to-year variability can be of order 0.1 optical depth units. A second reason for the discrepancies may be explained by the fact that the satellite-retrieval algorithms have been optimized for open-ocean areas, whereas the AERONET measurements at some of these locations may sense aerosols from mixed, polluted, and open-ocean sources. Finally, the aerosol retrievals refer to optical depths inferred for a 1° by 1° area, whereas the AERONET measurements are point data that refer to a specific point within each region covered by the retrieval data.

As noted above, a second method for determining aerosol abundance has been to compare retrieved broadband reflected solar irradiance with that determined from models. Haywood et al. (1999) used this method to infer the contribution of sea salt aerosols to total reflectivity. Monthly mean irradiances from the ERBE satellite over oceanic regions were computed for data from July 1987 to December 1988. This method relies on the difference between the observed clear-sky irradiance and that of a model calculation of the clear-sky irradiance without the effect of aerosols to determine the effects of aerosols on reflected flux. Thus, this method relies on an accurate parameterization of ocean surface albedo. The difference between the model-derived reflectivity with aerosols and that derived from ERBE can be used to judge the accuracy of model calculations of aerosols. Fortunately, ERBE shortwave radiances are calibrated to within 2%–3%. However, the cloud-screening algorithm used for the ERBE analysis may lead to overestimates of the clear-sky shortwave flux. Perhaps because of this, ERBE clear-sky fluxes are higher than those derived from the Clouds and Earth's Radiant Energy System (CERES) instrument (which has smaller pixels) by an average of 15% (N. Loeb 2000, personal communication). Thus, this may lead to a diurnal-average error of order 6 W m^{-2} associated with the cloud screening algorithm of ERBE. In determining reflectance from the models, we followed the Haywood et al. procedure and used monthly mean aerosol abundances

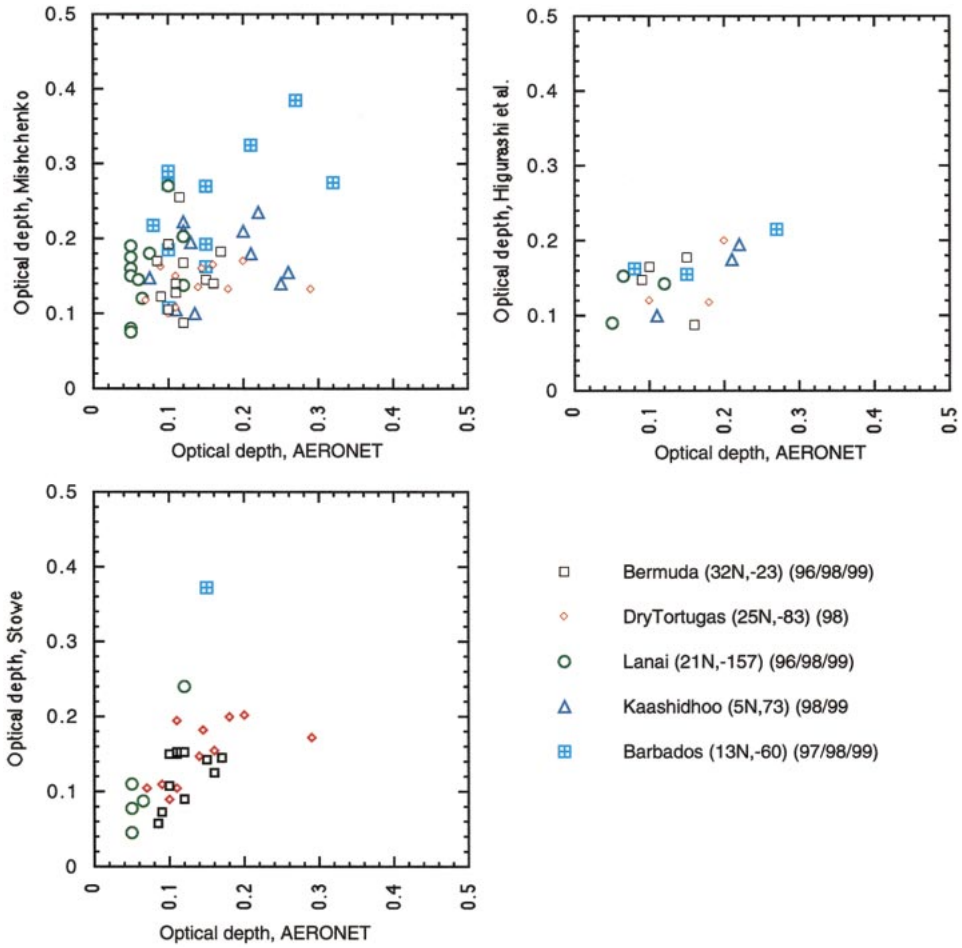

FIG. 1. Comparison of monthly average optical depth at 0.55 μm measured by sun photometer at different marine locations within the AERONET network and that derived for the same location from the analysis of (a) Mischenko et al. (1999), (b) Higurashi et al. (2000), and (c) Stowe et al. (1997). Only 4 months of data are shown for the comparison in (b). The time period covered by the AERONET observations at each station are shown in the key to symbols.

and assumed aerosol optical properties for 80% relative humidity. In addition, there was no attempt to account for differences in the influence of varying water vapor on clear-sky irradiance. Also, whereas in the original analysis from Haywood et al. (1999), the vertical structure of aerosol concentration from the Geophysical Fluid Dynamics Laboratory (GFDL) model was used, for this analysis, the vertical structure for each model was assumed to be that from the GFDL model. Such differences may not matter since the RH dependence of aerosol scattering is not accounted for.

The models considered here were those that participated in the IPCC model intercomparison (Penner et al. 2001). Only those models that included the full suite of aerosol types are considered here. The models and relevant references are listed in Table 1. A seventh model, that from the Pacific Northwest National Laboratory, provided aerosol concentrations from all the major aerosol types. However, the modeled dust concentrations did not include the supermicron dust sources and their modeled sea salt concentrations were significantly lower than those from the other models. Hence, their modeled optical depths were significantly smaller than those from the models represented here and are not considered further.

The emissions specified for the model simulations reported here were as follows. Anthropogenic sulfur emissions used the draft IPCC-specified 2000 scenario (Nakicenovic et al. 2000) and totaled 69 Tg-S yr^{-1}. We note that these emissions have a significantly larger portion of their total emissions associated with Southeast Asia in contrast to emissions developed for the year 1985 (see, e.g., Benkovitz et al. 1996) which are closer to the time period of analyzed satellite data. The dimethylsulfide (DMS) fluxes were generated from the ocean DMS field compiled by Kettle et al. (1999) and totaled 25.3 Tg-S yr^{-1}. Volcanic SO_2 sources were from Andres and Kasgnoc (1998; 9.6 Tg-S yr^{-1}). Organic aerosols from ter-

TABLE 1. Aerosol models participating in optical depth intercomparison.

Code	Model	Contributor	Reference
1	ULAQ	Pitari	Pitari et al. (2001); Pitari and Mancini (2001)
2	GISS	Koch and Tegen	Koch et al. (1999); Tegen and Miller (1998)
3	GOCART (Georgia Institute of Technology–GSFC)	Chin and Ginoux	Chin et al. (2000); Ginoux et al. (2001)
4	CCMI–GRANTOUR (Lawrence Livermore National Laboratory–University of Michigan)	Chuang, Penner, and Zhang	Chuang et al. (1997); Chuang et al. (2000, manuscript submitted to *J. Geophys. Res.*)
5	ECHAM 4.0 (MPI–Dalhousie)	Feichter, Land, and Lohmann	Feichter et al. (1996); Lohmann et al. (1999)
6	ECHAM 3.6–GRANTOUR (University of Michigan)	Herzog, Penner, and Zhang	Penner et al. (2001)

penes totaled 14.4 Tg yr^{-1} and were generated from the inventory provided by Guenther et al. (1995). Organic carbon and black carbon aerosols from fossil fuels were treated together with biomass aerosols and were developed from the inventories of Penner et al. (1993) and Liousse et al. (1996). These totaled 81.4 Tg yr^{-1} and 12.4 Tg yr^{-1}, respectively and were developed for calendar year 1980. Dust aerosols were generated using the algorithm described by Ginoux et al. (2001) for winds from 1990 and totaled 400 Tg yr^{-1} for $D < 2$ μm and 1750 Tg yr^{-1} for $D > 2$ μm. Finally, sea salt aerosols were generated using the algorithm described by Gong et al. (1997) and totaled 88.5 Tg-Na yr^{-1} for $D < 2$ μm and 1066 Tg-Na yr^{-1} for $D > 2$ μm.

In examining the comparisons of optical depth between the models, and between the models and the data, it should be noted that two models did not follow the specifications for the IPCC workshop. The Georgia Institute of Technology–Goddard Space Flight Center (GSFC) global ozone chemistry aerosol radiation transport (GOCART) model used a source distribution for sea salt that was derived from daily varying Special Sensor Microwave Imager (SSM/I; Atlas et al. 1996) winds for 1990 and was, on average, 55% larger than the baseline sea salt source specified for the model workshop. While this source may be more realistic than the workshop-specified source (because it used satellite-derived winds rather than model-derived winds) it was not available to all participants to use. Additionally, the Max Planck Institude (MPI)–Dalhousie University model used dust and sea salt distributions that were derived from a previous simulation of the (CCM1) Community Climate Model–GRANTOUR model (Lohmann et al. 1999).

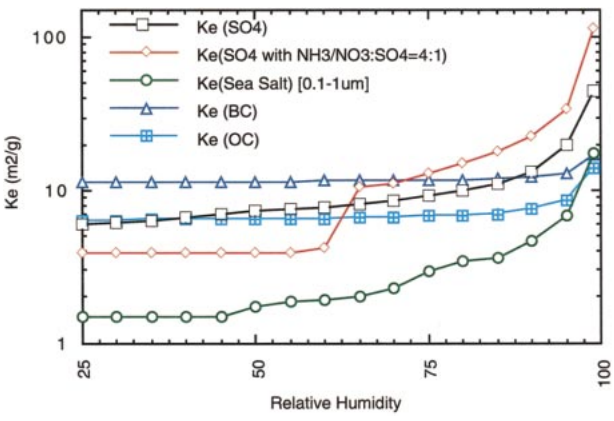

FIG. 2. Extinction coefficient for sulfate and submicron sea salt aerosol used in the offline analysis of optical depth (black square and green diamond). The values used for sulfate for the sensitivity study (determined assuming a molar ratio of NH_3 and HNO_3 of 4 to 1 relative to sulfate; red diamond) and the values for the sensitivity study for black carbon and organic carbon (blue triangle and blue square, respectively) are also shown.

3. Aerosol optical properties

Determination of aerosol optical depth from column aerosol mass usually proceeds with first determining an assumed aerosol size distribution, followed by the determination of dry aerosol scattering and absorption cross sections together with a factor showing how these properties change as a function of relative humidity. Here, spherical particles are assumed so that Mie scattering may be used to calculate the aerosol optical properties. For internal mixtures of compounds (such as water associated with sulfate aerosols) the refractive indices were volume-weighted. Effects of changes in the real part of the refractive index are particularly important at high relative humidity.

The amount of water associated with the aerosol depends on the chemical nature of the aerosol. Several of the models that participated in our study determined optical depth in line, that is, from instantaneous variations in model-determined relative humidity and aerosol abundance. However, in order to sort out differences caused by differences in humidity among the models as well as differences in aerosol properties, we developed an offline analysis of aerosol optical depth from the reported monthly averaged three-dimensional fields of aerosol concentrations from each model.

Aerosol properties specified in our offline calculation for the different aerosol types are shown in Fig. 2 and values at 80% relative humidity are reported in Table 2. The figure shows the extinction cross section per unit aerosol mass (i.e., the specific extinction cross section, K_e) for different particles as a function of relative humidity between 25% and 100%. The values for sulfuric

TABLE 2. Extinction coefficients at 0.55 μm and 80% relative humidity used in this analysis and in each models' inline calculation of optical depth.

Model	Sulfate	Organic carbon	Black carbon	Dust r = (0.1–1.0 μm)	Dust r = (1.0–10 μm)	Sea salt r = (0.1–1.0 μm)	Sea salt r = (1.0–4.0 μm)	Sea salt r = (4–10 μm)
This analysis, base case	9.94[a]	8.04	9.26	1.5	0.3	3.45[a,b]	0.69[a,b]	0.20[a,b]
Values at 80% RH used for reflectivity	9.74	8.04	9.26	–[c]	–[c]	2.5	2.5	2.5
ECHAM–GRANTOUR	12.2	7.4	9.6	1.13	0.45	2.83[a]	1.27[a]	1.27[a]
ULAQ	7.35[a]	3.67	8.90	1.23	0.49	1.45	0.48	0.12
GISS	8.56[a]	8	9	–[d]	–[d]	2.0	2.0	2.0
GOCART	10	8	10	–[e]	–[e]	0.4	0.4	0.4

[a] Indicates that these were included in the analysis with a humidity dependence.

[b] The total mass- and size-weighted average extinction coefficient for sea salt from our analysis assuming the size distribution from Quinn et al. (1998) is 2.4 $m^2\ g^{-1}$.

[c] The analysis of optical depth in our study of reflectivity scaled the total mass of dust from each model to the vertical profile used in the study of Haywood et al. (1999). The following values for K_e for dust were used:

r_e (μm)	K_e ($m^2\ g^{-1}$)
0.1	1.7
0.2	3.2
0.4	2.4
0.8	0.91
1.0	0.74
2.0	0.34
4.0	0.16
8.0	0.08

[d] The GISS model used the following values for dust:

r_e (μm)	K_e ($m^2\ g^{-1}$)
0.1	4.77
0.2	4.22
0.4	2.32
0.8	0.97
1.5	0.47
2.5	0.27
4.0	0.09

[e] The GOCART model used the following values for dust:

r_e (μm)	K_e ($m^2\ g^{-1}$)
0.14	3.29
0.24	3.52
0.45	2.06
0.8	0.97
1.4	0.47
2.4	0.26
4.5	0.14

acid aerosols were determined for H_2SO_4 in equilibrium with water vapor at the stated relative humidity and a temperature of 275 K. The size distribution followed assumptions in Chuang et al. (1997) for continental aerosols. The aerosol models that participated in this intercomparison study did not explicitly include ammonium or nitrate in aerosols. Inclusion of these components can significantly increase the extinction cross section when calculated relative to the sulfate (SO_4^{2-}) in the aerosol. Therefore, to examine the effects of changes in composition, we also considered a sensitivity case in which we calculated the effect of also adding NH_3 and HNO_3 to the system. These were specified with molar ratios of 4 to 1 relative to sulfate based on the results of chemical transport models (Dentener and Crutzen 1994; Penner et al. 1994). The specific extinction cross section for the base case is 9.94 m^2 g $(SO_4^{2-})^{-1}$ at 80% relative humidity while that of an aerosol in equilibrium with a 4 to 1 ratio of HNO_3 and NH_3 to SO_4^{2-} is 15 m^2 g $(SO_4^{2-})^{-1}$. These values increase to 44.0 m^2 g $(SO_4^{2-})^{-1}$ and 113 m^2 g $(SO_4^{2-})^{-1}$, respectively, at 99% relative humidity.

The extinction caused by carbonaceous particles is poorly known. In the absence of better information, for our base case we simply used the values for 80% relative humidity specified by Haywood et al. (1999; see Table 2). However, we also examine a case in which we used the size distribution and the fit to the growth rate associated with the measured response of biomass burning aerosols to changes in humidity (Penner et al. 1998). This leads to values of 11.4 m^2 g (aerosol)$^{-1}$ and 6.41 m^2 g (aerosol)$^{-1}$ for black carbon and organic carbon

at 40% relative humidity, respectively, increasing to values of 16.9 m^2 g (aerosol)$^{-1}$ and 13.7 m^2 g (aerosol)$^{-1}$, respectively, at 99% relative humidity.

The extinction cross sections for sea salt were derived using the size distribution from Quinn et al. (1998) assuming that the composition was that of NaCl in equilibrium with water vapor at the stated relative humidity. To avoid the effects of the dilequescent behavior of NaCl, between 45% and 85% relative humidity, we applied the growth factor derived from the clean marine measurements reported by Carrico et al. (1998), while above 85% relative humidity we again used the model-calculated results for NaCl in equilibrium. Applying the mass distribution for each size range yields an average mass-weighted extinction cross section of 2.4 m^2 g (NaCl)$^{-1}$ at 80% relative humidity, a value similar to that used in our analysis of reflectivity (see Table 2). Values for dust were constant as a function of relative humidity and were derived from Tegen et al. (1997).

To derive optical depth from each model, we first summed their mass mixing ratios as a function of aerosol size to the size bins used here for K_e. Then we calculated the optical depth from the frequency distribution of the vertical profile of relative humidity, the product of K_e at each humidity, and the monthly average concentration profile. The relative humidity was determined from the ECMWF–Hamburg (ECHAM) 3.6 climate model. These model-derived relative humidity fields compare favorably to the relative humidity fields derived from the European Centre for Medium-Range Weather Forecasts (ECMWF) model though they are somewhat drier than the ECMWF model. The mean relative humidities are within 3% at the surface although they differ by 7% at 925 mb. The root mean square deviation between the model-derived and ECMWF-derived relative humidities is less than 20% at all levels below 250 mb and less than 10% below 950 mb. As the last step in deriving optical depth, we formed a vertical integral to determine optical depth at each latitude and longitude. The optical depths compared here to those from the satellites are those derived over the ocean areas.

The values used for the inline calculation at 80% relative humidity by each model are also summarized in Table 2. Also shown are the values used in our analysis of reflectivity by each model (see Haywood et al. 1999).

The use of different treatments for the optical parameters as well as relative humidity treatments in the models led to substantial differences in the derived inline optical depths compared with those from our offline calculation. This is shown in Fig. 3, which compares the over-ocean optical depths derived from each inline calculation (where reported) with those from our offline calculation. As shown there, the University of L'Aquila (ULAQ) and GOCART inline versions of optical depth are significantly lower than that from the offline case. This is mainly due to the use of a lower sea salt extinction coefficient that did not account for the humidity dependence of sea salt extinction (see Table 2). The Goddard Institute for Space Studies (GISS) inline version of optical depth is close to our offline analysis but is also somewhat lower. In the case of the GISS model, differences in relative humidity may account for the differences in optical depth. Because of these differences, in our comparison to satellite-retrieved optical depth, we concentrated on calculations that used our offline calculation of optical depth. Subsequent calculations showed that the offline procedure produced monthly average optical depths that were similar to those determined in the inline version of the ECHAM–GRANTOUR model when similar extinction cross sections are used.

To examine the differences caused by our use of constant values for the specific extinction coefficient in the analysis of reflectivity, Fig. 3 also compares the optical depth calculated over the ocean based on this assumption with that derived from our offline calculation. As shown there, for most models, the evaluation of optical depth using the assumption of 80% relative humidity leads to an overestimate of optical depth relative to that calculated from the frequency distribution of relative humidity. The amount of the overestimate ranges up to 0.2 for the GISS model in January. The relative humidity from the ECHAM model is slightly lower than 80% on average (i.e., it is 73% and 74% at 1000 mb in January and July, respectively, and decreases to 59% and 64%, respectively, at 925 mb). The corresponding values for the ECMWF average fields are 77% and 73% at 1000 mb in January and July, respectively, and 76% and 72% at 925 mb in January and July, respectively.

4. Comparison of the models with AVHRR-derived optical depth

The optical depth at each location is the sum of the optical depths determined for each aerosol type. In order to sort out the importance of different aerosol components to the longitudinal average optical depth over oceans, Fig. 4 presents the contribution of each aerosol component to the zonal average cumulative optical depth determined from the offline calculation for the ECHAM–GRANTOUR model for January, April, July, and October. The figure also shows the retrieved optical depths from the AVHRR satellite analysis of Higurashi et al. (2000; labeled result: 1 and result: 2), Mischenko et al. (1999), and Stowe et al. (1997). The GRANTOUR model was chosen to highlight for this analysis because its individual components were in reasonable agreement with the surface observations of aerosol components. However, several of the other models were in similar agreement with the data (Penner et al. 2001).

The optical depth north of 40°N is determined mainly by sea salt in January and April with the second most important component being sulfate. In July the dominant component is sulfate, with contributions from dust and

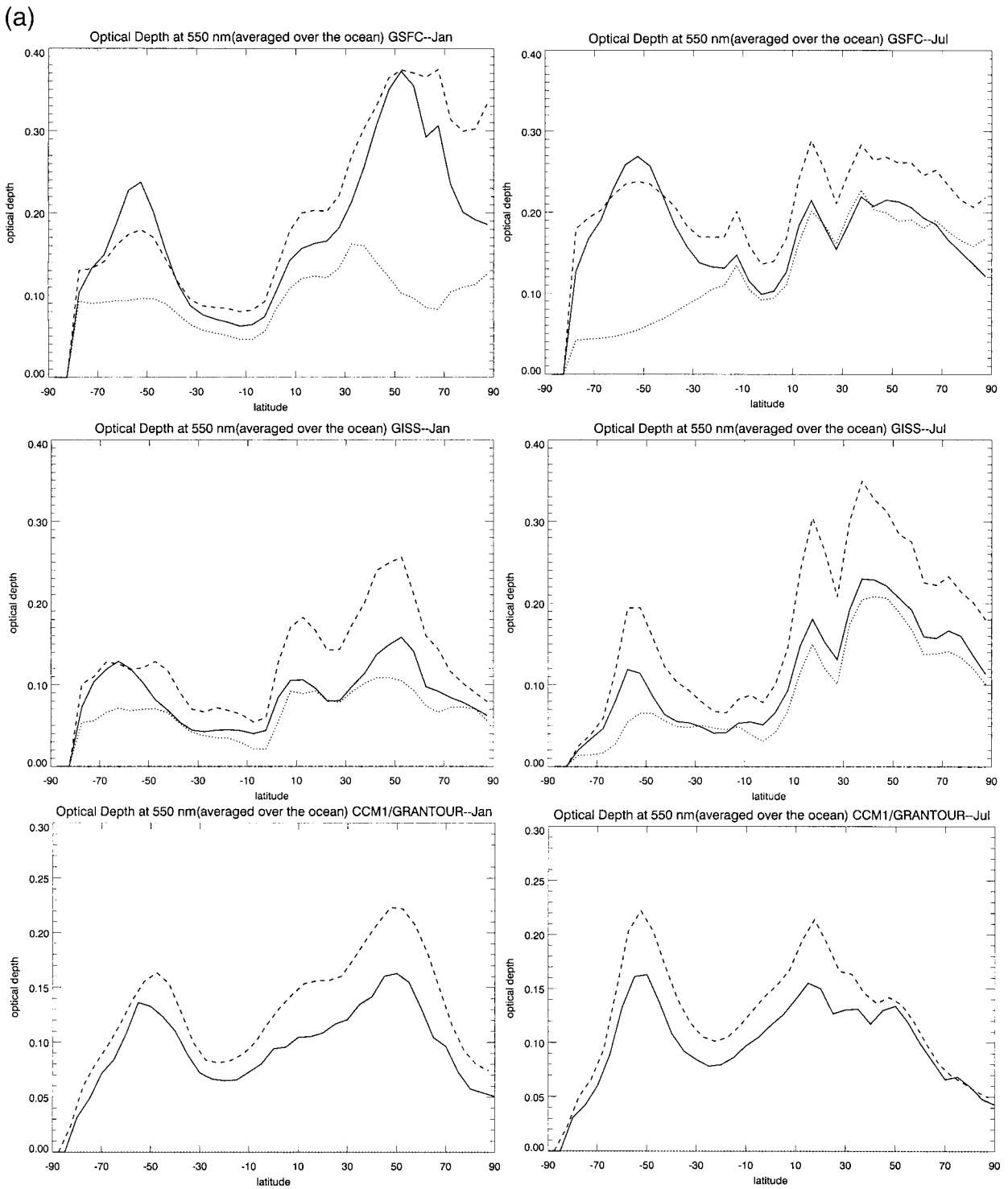

FIG. 3. Aerosol optical depths over the ocean for Jan and Jul derived for the offline calculation based on the assumed distribution of different relative humidities (solid line), based on the assumed optical extinction coefficients at 80% RH (dashed line), and based on the inline calculation from each model if available (dotted line).

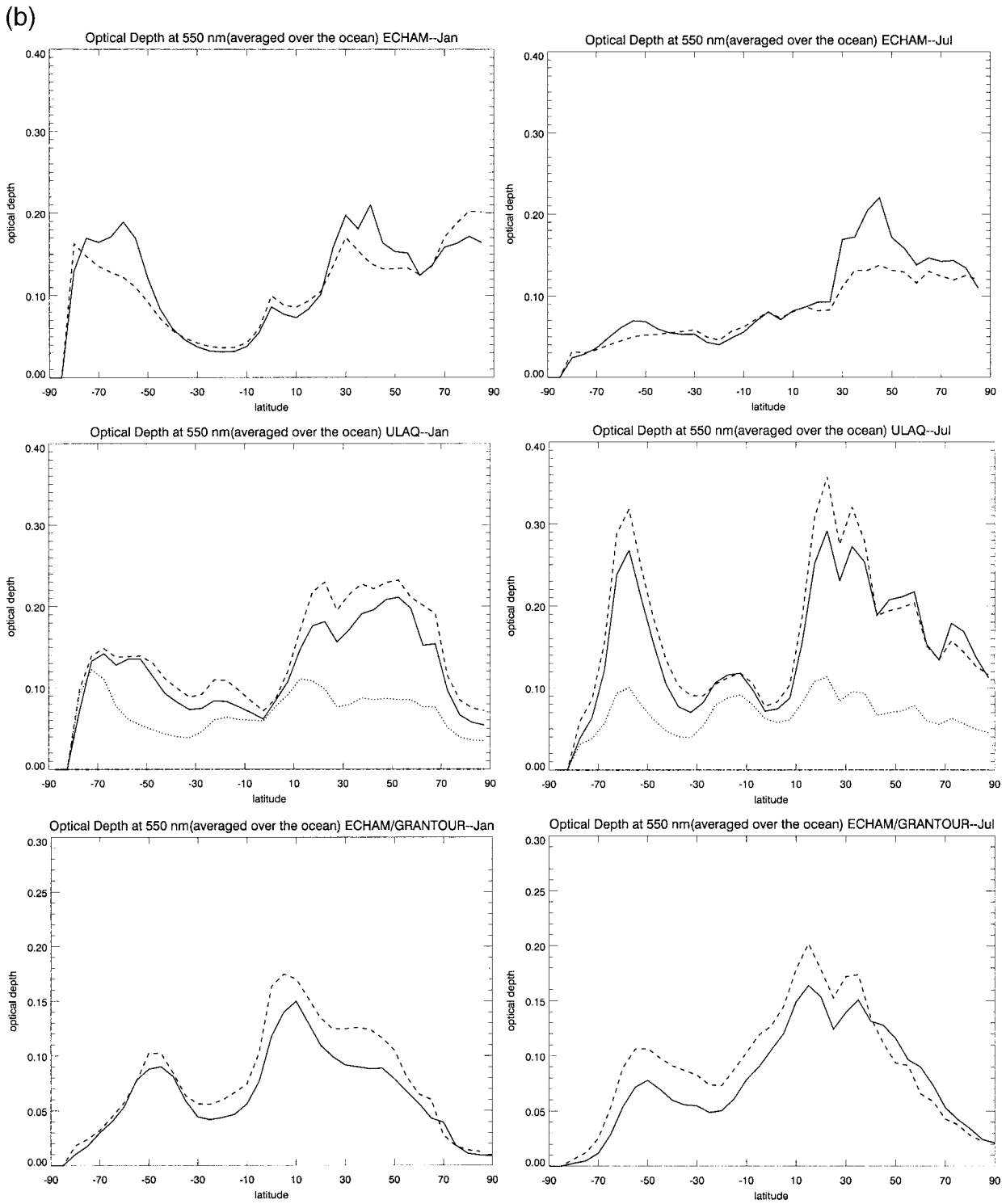

FIG. 3. (*Continued*)

sea salt that are each of order 25% of the total optical depth. In October, sea salt is again the most dominant contributor but sulfate and dust are also important (≈10%–20%).

The local maximum in modeled optical depth near 10°N in January and April is associated with sulfate, dust, and organic and black carbon. The local maximum is centered near 15°N in July and October, when dust

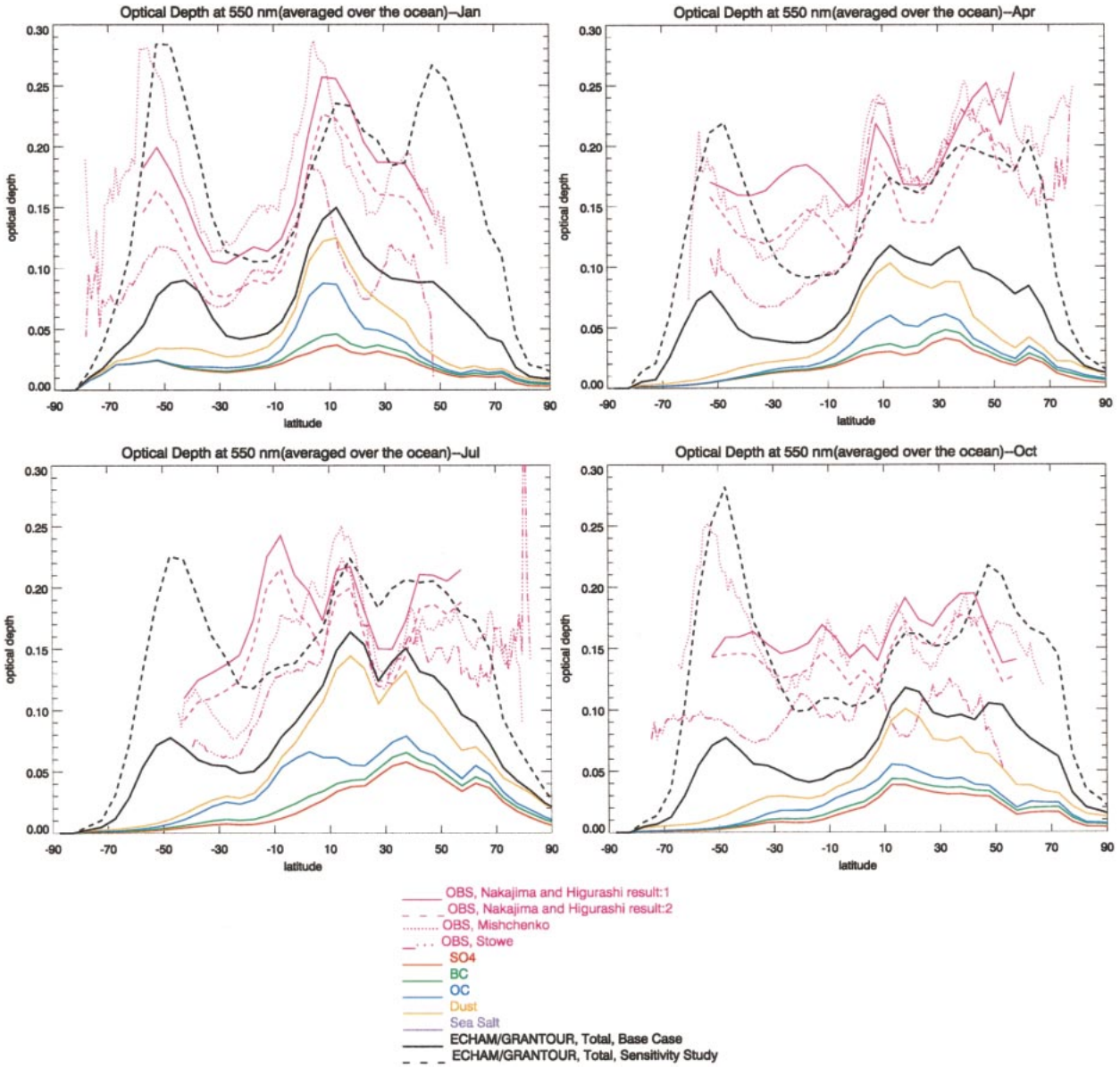

FIG. 4. Contribution of different aerosol types to the zonal average cumulative optical depth in (a) Jan, (b) Apr, (c) Jul, and (d) Oct for the ECHAM–GRANTOUR base case optical properties and fluxes. The purple line for the addition of sea salt overlies the total optical depth for the base case. The total for the sensitivity study is also shown. The aerosol optical depths derived from the analysis of Higurashi et al. (2000) and Nakajima and Higurashi (1998; labeled result:1 and result:2), Mishchenko et al. (1999), and Stowe et al. (1997) are also shown.

appears to contribute most to this peak, with a secondary contribution by sulfate.

Between 10° and 30°S, there is a local minimum in the model- and satellite-derived zonal average optical depth in January. Sulfate, dust, and sea salt all contribute to the optical depth here. In April there is a local maximum in retrieved optical depth from Higurashi et al. (2000) near 20°S, but the model-calculated optical depth and the other two retrievals do not reproduce this maximum (though there is a flattening of the curves in the two other retrievals). In July there is a local maximum in retrieved optical depth near 10°S, which is also not present in the model. Finally, in October there is a local maximum in retrieved optical depth near 15°S that is again not present in the model.

Near 50°S, there is a local maximum in zonal average retrieved optical depth that is evident in all months in the retrieved data. This peak is also present in the model and is associated with sea salt.

As noted in Fig. 4, the derived optical depths from the ECHAM–GRANTOUR model for the base case are, in most cases, less than those derived from the analysis of AVHRR. In order to explore the source of this bias, we examined the sensitivity of the derived optical depth

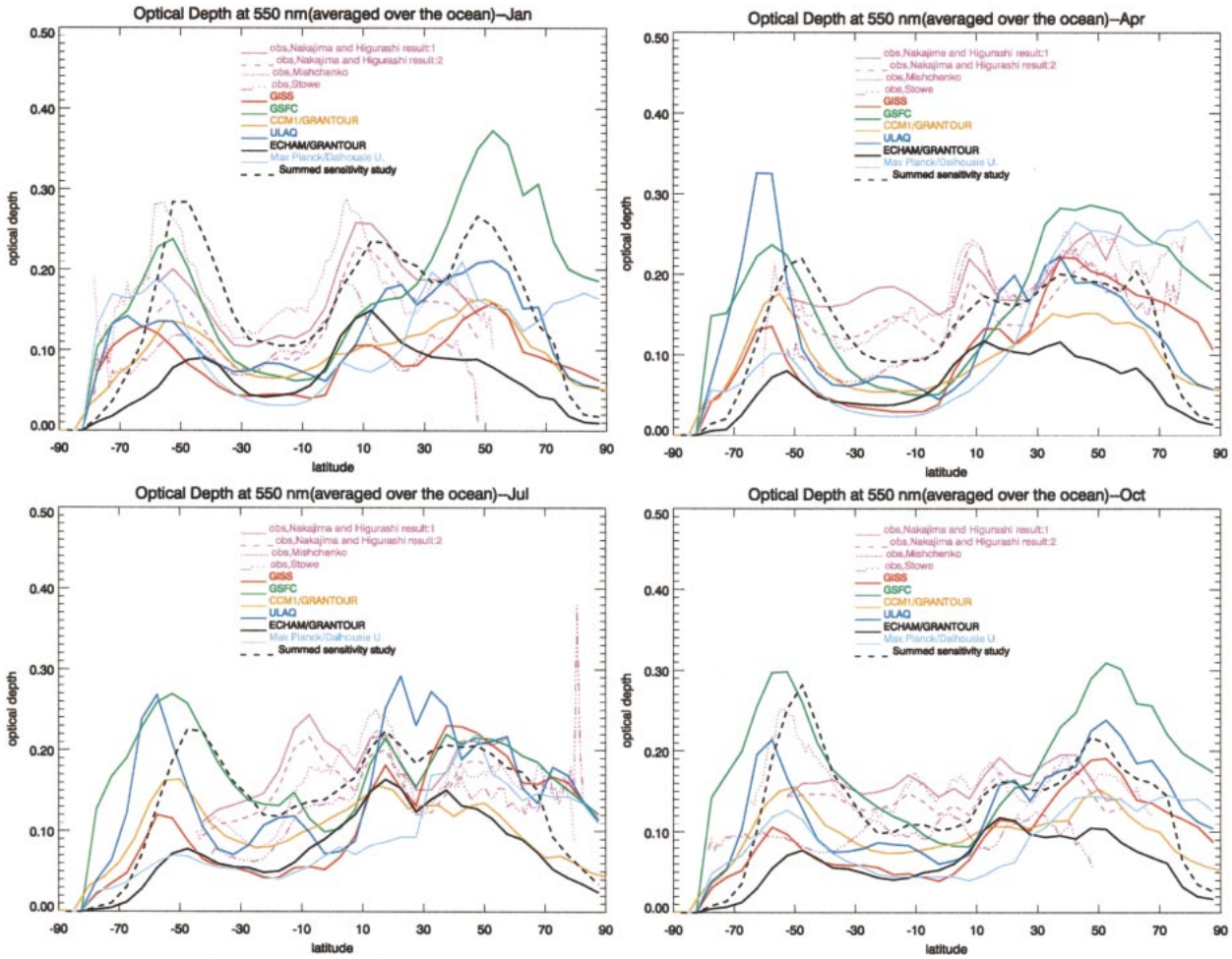

FIG. 5. Aerosol optical depth derived from AVHRR satellite analysis following Higurashi et al. (2000) and Nakajima and Higurashi (1998; labeled result:1 and result:2), Mishchenko et al. (1999), and Stowe et al. (1997) for Jan, Apr, Jul, and Oct. The results from Nakajima refer to 1990, while those from Mishchenko and Stowe refer to an average over the years 1985–88. The results derived from the models that participated in the IPCC-sponsored workshop are also shown. The case labeled ''summed sensitivity study'' shows the derived optical depth for the ECHAM–GRANTOUR model using a factor of 2 increase in the DMS flux; the monthly average sea salt fluxes derived using the SSM/I wind fields; and the extinction coefficients for organic carbon, black carbon, and SO_4^{2-} from the sensitivity case shown in Table 2.

to changes in both the sources of the aerosols as well as their optical properties. These changes all conspire to increase optical depths, but, except for the change in DMS flux, may have been biased low in the base case (see discussion above). We considered the variation in the extinction coefficient for SO_4^{2-} that results from the assumption that SO_4^{2-} was in equilibrium with a 4 to 1 ratio of HNO_3 and NH_3 to SO_4^{2-}. The behavior of organic carbon and black carbon as a function of relative humidity was derived assuming that 30% of the composition was ammonium sulfate (Penner et al. 1998). Also, for the sensitivity case, the flux of DMS was increased by a factor of 2 and the monthly average sea salt fluxes derived for the GOCART simulation were used. As noted above, these latter fluxes were, on average, 55% larger than those in the base case. In most months and at most latitudes more than 50% of the increase in optical depth in the sensitivity case was associated with the increased fluxes of DMS and sea salt. In July at Northern Hemisphere midlatitudes, the change in optical properties is more important and the percentage increase explained by the increase in fluxes is only 30%.

Figure 4 also presents the total optical depth from the sensitivity case. The optical depths from the sensitivity case are, in all cases, much closer to the retrieved values of optical depth than are the optical depths from the base case. However, in April, between 10° and 30°S, and in July and October near 10°S, the modeled optical depth is still less than that deduced from the Higurashi et al. (2000) and Mishchenko et al. (1999) analyses.

Figure 5 shows the calculated offline values of zonal average aerosol optical depth in January, April, July, and October from each of the models in the IPCC intercomparison together with the retrieved optical depth from the analyses of Mishchenko et al. (1999), Higur-

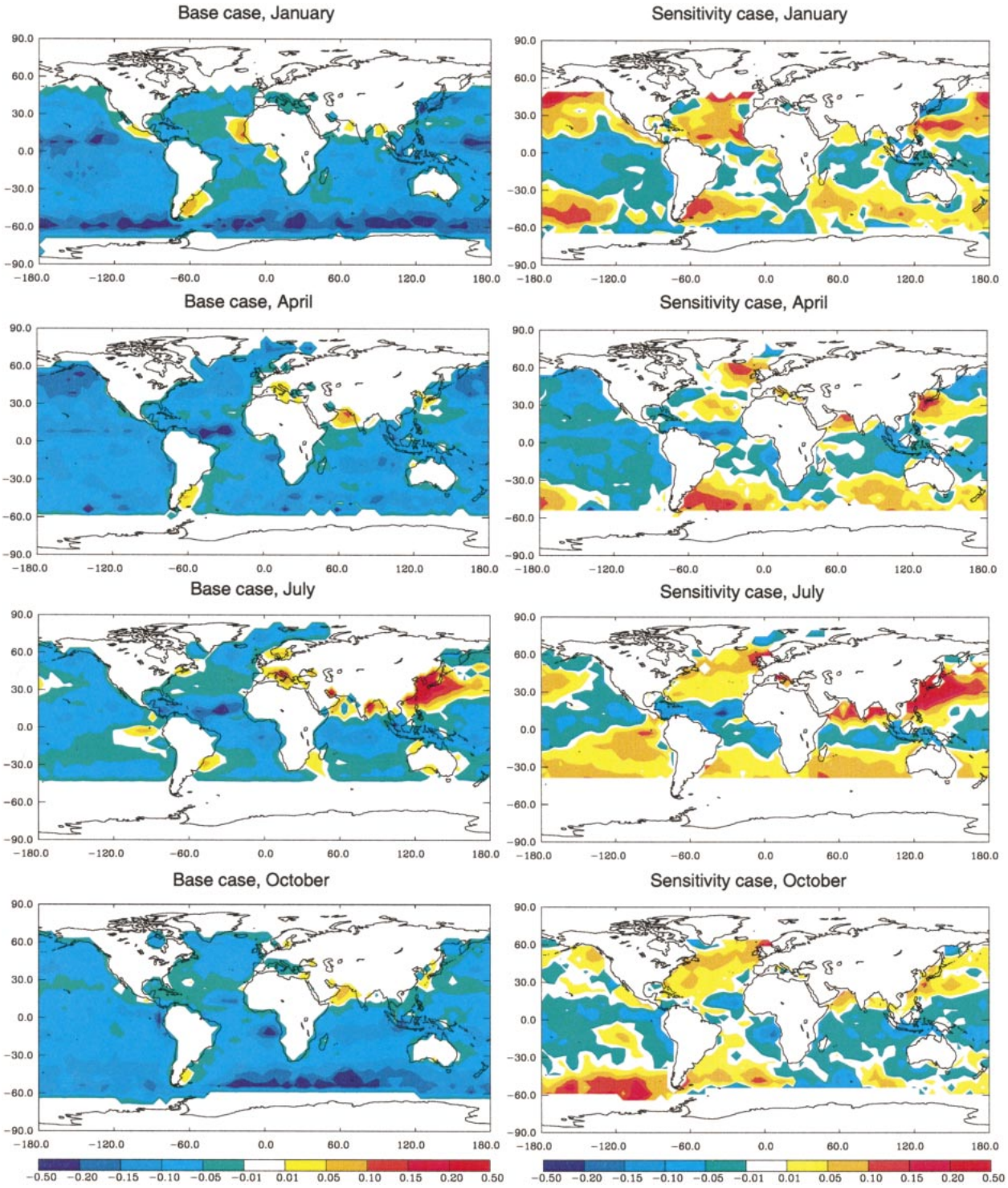

FIG. 6. Difference between the ECHAM–GRANTOUR computation of optical depth and the satellite-retrieved optical depths from Mishchenko et al. (1999). The left column shows the optical depths derived for the standard set of sources, while the right panel shows the derived optical depths for the sensitivity study using a factor of 2 increase in the DMS flux and the monthly average sea salt fluxes derived using the SSM/I wind fields and high optical extinction coefficients for SO_4^{2-} and carbon aerosols (see text). Note that the anthropogenic sulfate sources were for the year 2000 while the satellite analysis covers the time period 1985–88. This may explain the systematic overestimate of optical depth off the coast of Asia in Jul.

TABLE 3. Difference between model-derived optical depth and that for each satellite-retrieved optical depth for Jan, Apr, Jul, and Oct. The difference between the model 4-month average and the satellite retrieval is also shown. The results for Nakajima are those for result:2 in Figs. 4 and 5. The result labled ''Model mean'' used the average value from all the models.

	Nakajima		Mishchenko		Stowe	
	Absolute error	Overall bias	Absolute error	Overall bias	Absolute error	Overall bias
Jan						
CCMI–GRANTOUR	0.05	−0.03	0.08	−0.08	0.03	0.00
ULAQ	0.06	−0.02	0.09	−0.07	0.05	0.01
MPI–Dalhousie	0.07	−0.05	0.10	−0.09	0.06	−0.01
GISS	0.06	−0.06	0.11	−0.11	0.04	−0.03
ECHAM–GRANTOUR	0.05	−0.05	0.10	−0.10	0.03	−0.02
GOCART	0.05	0.01	0.07	−0.03	0.06	0.04
Model mean	0.04	−0.03	0.09	−0.08	0.04	0.00
Apr						
CCMI–GRANTOUR	0.06	−0.05	0.07	−0.07	0.05	−0.04
ULAQ	0.07	−0.03	0.08	−0.05	0.05	−0.03
MPI–Dalhousie	0.08	−0.06	0.09	−0.08	0.06	−0.05
GISS	0.08	−0.06	0.09	−0.08	0.05	−0.05
ECHAM–GRANTOUR	0.07	−0.07	0.09	−0.09	0.06	−0.06
GOCART	0.07	−0.01	0.07	−0.03	0.05	0.00
Model mean	0.06	−0.05	0.07	−0.07	0.04	−0.04
Jul						
CCMI–GRANTOUR	0.05	−0.04	0.05	−0.03	0.03	−0.01
ULAQ	0.08	−0.01	0.08	0.00	0.06	0.02
MPI–Dalhousie	0.09	−0.07	0.08	−0.06	0.07	−0.04
GISS	0.08	−0.05	0.08	−0.04	0.06	−0.02
ECHAM–GRANTOUR	0.07	−0.05	0.06	−0.04	0.04	−0.02
GOCART	0.07	0.01	0.07	0.01	0.06	0.03
Model mean	0.06	−0.03	0.06	−0.03	0.04	−0.01
Oct						
CCMI-GRANTOUR	0.04	−0.03	0.06	−0.05	0.03	0.01
ULAQ	0.06	−0.02	0.07	−0.04	0.05	0.02
MPI–Dalhousie	0.07	−0.06	0.09	−0.08	0.04	−0.02
GISS	0.07	−0.05	0.09	−0.08	0.04	−0.01
ECHAM–GRANTOUR	0.06	−0.06	0.09	−0.09	0.03	−0.02
GOCART	0.06	0.03	0.06	0.01	0.09	0.08
Model mean	0.05	−0.03	0.06	−0.05	0.03	0.01
4-month average						
CCMI–GRANTOUR	0.05	−0.04	0.07	−0.06	0.04	−0.01
ULAQ	0.07	−0.02	0.08	−0.04	0.05	0.00
MPI–Dalhousie	0.08	−0.06	0.09	−0.08	0.06	−0.03
GISS	0.07	−0.05	0.09	−0.07	0.05	−0.03
ECHAM–GRANTOUR	0.06	−0.06	0.09	−0.08	0.04	−0.03
GOCART	0.06	0.01	0.07	−0.01	0.07	0.04
Model mean	0.05	−0.04	0.07	−0.06	0.04	−0.01

ashi et al. (2000), and Stowe et al. (1997). Table 3 reports the absolute difference and bias between the 4-month average optical depth determined for each model and the analysis of Higurashi et al. (2000), Mishchenko et al. (1999), and Stowe et al. (1997), respectively; and Table 4 reports the overall bias by latitude. Because the GISS, CCM1, ECHAM–GRANTOUR, and ULAQ models all used the same sources, the differences between these models are mainly due to model parameterization procedures for precipitation scavenging. There were also large differences in the vertical distribution of aerosol mixing ratios (Penner et al. 2001).

To derive a quantitative comparison of the differences among retrieved values and between the retrieved values and the models, the optical depths shown in Fig. 5 were averaged in 10° latitude bins (see Table 4). Turning first to the comparison of retrieved optical depths, we note that the different satellite-derived optical depths differ by between −0.10 and 0.07 optical depth units in comparison to the average of the three analyses depending on latitude and month, but the general features of the retrievals are similar. The satellite-derived optical depths from Stowe et al. (1997) are lower on average by 0.05 and by 0.03 than those from Mischenko et al. (1999) and from result:2 from Higurashi et al. (2000), respectively. The latter two retrievals make use of a 2-wavelength technique, which is thought to be more accurate than the 1-wavelenth technique of Stowe et al.

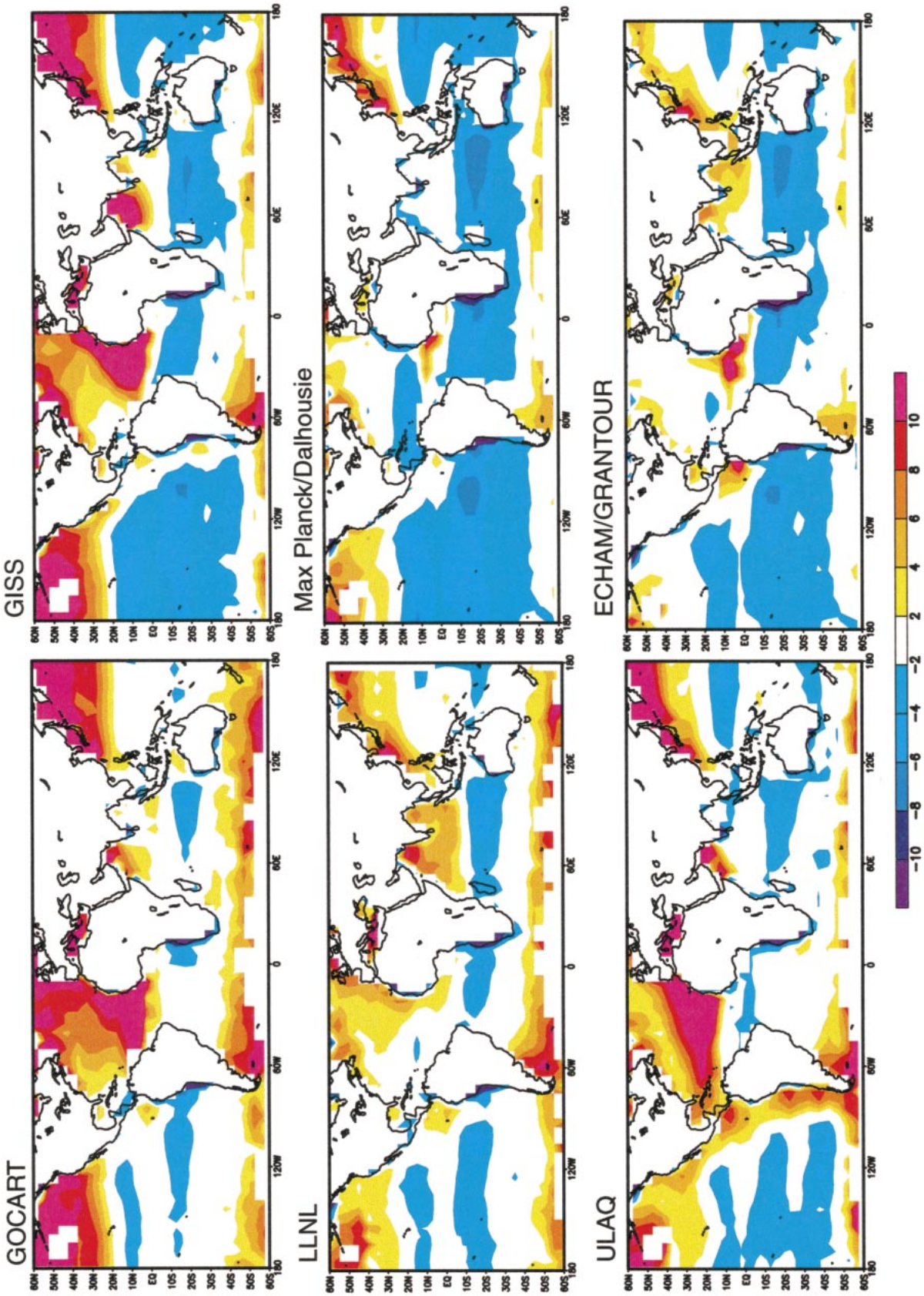

(1997). However, it is worth bearing in mind that most of the difference in retrieved aerosol optical depth may be related to cloud screening techniques (Mishchenko et al. 1999) or to assumed size distribution (Higurashi et al. 2000).

To ease comparison with measurements and to gauge the range of results associated with the different models, for the model analysis, we formed the average optical depth over all the different models. The individual modeled optical depths differ by between −0.09 and +0.16 optical depth units from the average of the models. Moreover, the differences between the average of the models and the average of the satellites ranges over −0.11 and +0.05 optical depth units. Modeled optical depths north of 30°N are sometimes higher and sometimes lower than those of the retrieved AVHRR optical depths. For example, they range from an average difference of 0.13 in July for the ULAQ model in comparison to result:2 for Higurashi et al. (2000) to an average difference of −0.09 in January for the ECHAM–GRANTOUR model in comparison to the retrieved optical depths from Mishchenko et al. (1999). The modeled optical depths in the latitude band from 30° and 40°N are systematically too high in July. For example, the average of the modeled optical depths is larger than the satellite-derived optical depth of Nakajima, Mishchenko, and Stowe by an average by 0.06, 0.05, and 0.04, respectively. We note that sulfate and dust provide the largest components of optical depth in this region with sea salt providing the third most important component (cf. Fig. 4). The black dashed line shows the estimated optical depths from the ECHAM–GRANTOUR model with the larger sea salt fluxes deduced from the SSM/I winds, with doubled DMS flux, and with optical properties for an assumed ratio of total NH_3NO_3 to H_2SO_4 of 4 to 1. Comparison of these results with those of the retrieved optical depths shows that the uncertainties in these parameters lead to changes in optical depth that are of order 0.05 and that can be as large as 0.2.

As shown in Fig. 4, the modeled aerosol optical depths near 10°N are dominated by dust with some contribution from organic carbon and sulfate (especially in January and April). They are systematically lower (by, on average, 0.08) than the average retrieved optical depth. The discrepancy between modeled and retrieved optical depths in this region, however, would be reduced if the sea salt fluxes derived from SSM/I winds and larger DMS fluxes had been used.

As shown in Fig. 4, the modeled aerosol optical depths from 10° to 30°S are due to a combination of different aerosol types. They are systematically lower than the average of the retrieved optical depths by an average of 0.06 with biases ranging from −0.14 to 0.01 in January, from −0.12 to −0.02 in April, from −0.13 to 0.07 in July, and from −0.11 to 0.06 in October. As shown by the sensitivity study, much of the difference between the modeled and retrieved zonal average optical depths could be removed by using higher sea salt and DMS fluxes. However, the spatial character of the differences reveals that the cause of the discrepancies probably cannot be attributed to any single source. For example, Fig. 6 shows the difference between the base case and sensitivity case for the ECHAM–GRANTOUR and the optical depths retrieved by Mishchenko et al. (1999). For the base case, in January the differences are largest in the central Pacific Ocean and near 60°S. In April the differences appear largest in the North Pacific Ocean and in the Atlantic Ocean west of the Sahara. In July and October the differences are mainly to the east of Asia and west and east of the African continent and also near 60°S in October. (We note that the large overprediction of optical depth in both the base case and the sensitivity case off the coast of Asia in July may be due to the difference in simulated year and the year of the optical depth retrievals. The model simulations used anthropogenic sulfate emissions appropriate to 2000 while the retrievals refer to an average of 1985–88.) The sensitivity study optical depth alleviates many of the negative differences in the base case, but several areas are still underpredicted.

Modeled aerosol optical depths near 60°S are dominated by sea salt. This component appears to be reasonably well represented by the models, especially for the optical depth predicted using the SSM/I sea salt fluxes. However, if some of the other models had used

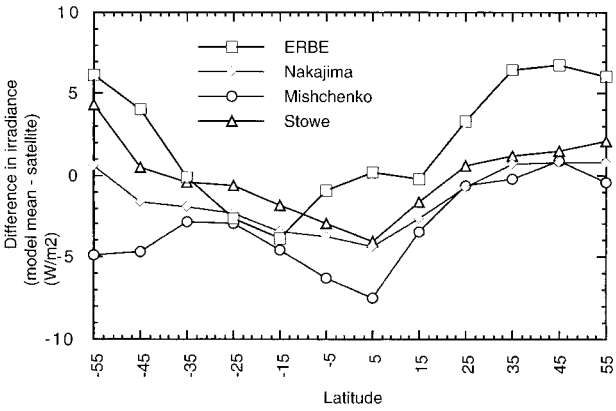

FIG. 8. Difference between the mean of the model predicted clear-sky shortwave flux and that from ERBE and from each of the AVHRR analyses.

←

FIG. 7. Difference between GCM computations and ERBE satellite observations of the annual mean solar irradiance reflected at the top of the atmosphere in clear skies over oceans for different models that participated in the IPCC model intercomparison: (a) GOCART, (b) GISS, (c) CCM1–GRANTOUR, (d) MPI–Dalhousie, (e) ULAQ, and (f) ECHAM–GRANTOUR models.

TABLE 4. Overall bias between the 4-month average model-derived optical depth and that for each satellite-retrieved optical depth (labeled O.D.) as a function of latitude. The calculated clear-sky shortwave flux difference (in W m^{-2}) is also given (labeled Flux). The results for Nakajima are those for result:2 in Figs. 4 and 5. Table 4a. Comparison with satellite retrieval of Mishchenko et al. (1999).

	CCMI–GRANTOUR		ULAQ		MPI–Dalhousie		GISS		ECHAM–GRANTOUR		GOCART		Mean of models	
Latitude	O.D.	Flux	O.D.	Flux	O.D.	Flux	O.D.	Flux	O.D.	Flux	O.D.	Flux	O.D.	Flux
−55.00	−0.06	−4.37	0.00	−1.18	−0.08	−6.07	−0.10	−7.89	−0.13	−10.84	0.04	1.93	−0.06	−4.91
−45.00	−0.06	−3.43	−0.08	−5.16	−0.09	−6.52	−0.11	−7.08	−0.11	−5.76	0.01	0.44	−0.07	−4.70
−35.00	−0.04	−2.06	−0.05	−3.01	−0.07	−4.54	−0.07	−4.25	−0.07	−3.46	0.01	0.17	−0.05	−2.89
−25.00	−0.04	−2.66	−0.03	−1.93	−0.07	−4.16	−0.07	−4.00	−0.07	−3.57	−0.01	−1.27	−0.05	−2.92
−15.00	−0.07	−4.41	−0.05	−3.07	−0.10	−5.91	−0.10	−5.85	−0.09	−4.83	−0.05	−3.48	−0.07	−4.55
−5.00	−0.08	−5.86	−0.09	−5.58	−0.11	−6.96	−0.12	−8.92	−0.08	−5.26	−0.08	−5.98	−0.09	−6.29
5.00	−0.11	−8.09	−0.13	−7.20	−0.14	−9.54	−0.13	−7.31	−0.09	−6.36	−0.11	−7.37	−0.12	−7.48
15.00	−0.08	−4.55	−0.03	−1.74	−0.12	−6.83	−0.07	−3.39	−0.07	−2.87	−0.05	−2.33	−0.07	−3.47
25.00	−0.03	−1.63	0.05	2.59	−0.04	−2.36	−0.03	−1.93	−0.03	−1.75	0.02	1.32	−0.01	−0.63
35.00	−0.04	−2.18	0.03	1.63	0.00	−0.20	−0.01	−0.76	−0.06	−3.05	0.05	2.96	0.00	−0.26
45.00	−0.03	−1.35	0.04	2.25	0.02	1.18	0.02	1.37	−0.07	−3.84	0.11	6.64	0.01	0.91
55.00	−0.05	−2.75	0.02	1.28	0.00	−0.45	0.00	0.33	−0.09	−6.83	0.08	4.82	−0.01	−0.47
Global average	−0.06	−3.76	−0.03	−2.00	−0.07	−4.64	−0.07	−4.32	−0.08	−4.64	0.00	−0.75	−0.05	−3.32

the higher fluxes used in the GOCART model, the optical depths would be overpredicted in this region.

Analysis of the AVHRR comparisons indicates that there is an overall bias between the average of the model-estimated optical depths and that from the AVHRR analysis of −0.02, −0.04, and −0.01 optical depth units in the Northern Hemisphere in comparison to the retrieved values of Higurashi et al. (2000) and Nakajima and Higurashi (1998), Mishchenko et al. (1999), and Stowe et al. (1997), respectively, and of −0.04, −0.07, and −0.01 optical depth units in the Southern Hemisphere, respectively. To further explore this issue, we next examine the reflectivity predicted from each of the models with the reflectivity measured by the ERBE satellite.

5. Comparison of models and measured shortwave reflection of solar radiation

Figure 7 shows the difference between the clear-sky reflected shortwave radiative flux from a model calculation using the GOCART, GISS, CCM1–GRANTOUR, MPI–Dalhousie, ULAQ, and ECHAM–GRANTOUR model-generated aerosols, and the ERBE-measured clear-sky fluxes. These figures were produced using the model-generated column aerosol burdens together with the modeled vertical aerosol distribution and extinction coefficients from Haywood et al. (1999; see their Table 1 and Table 2 in this paper). Table 5 shows the difference in clear-sky flux averaged over January, April, July, and October as a function of latitude.

The reflected shortwave flux north of 30°N is overpredicted by the ULAQ, GOCART, and GISS models by more than 8 Wm^{-2} and is also overpredicted (but to a lesser extent) by the MPI–Dalhousie and CCM1–GRANTOUR models. The ECHAM–GRANTOUR model does a good job of predicting the reflected flux in this region (but the values from the sensitivity test are too high). The comparison of annual average optical depth from the three models with highest reflected flux difference (ULAQ, GOCART, and GISS) models was also larger than the satellite-retrieved optical depths according to Stowe et al. (1997). The comparison of the two highest models (GOCART and ULAQ) with the optical depth from the Mishchenko et al. (1999) and Higurashi et al. (2000) optical depths is similarly too high, although the CCM1–GRANTOUR model, MPI–Dalhousie, and GISS are somewhat smaller than the retrieved optical depth from Mishchenko et al. (1999) and the CCM1–GRANTOUR optical depth is smaller than the retrieved optical depth from Higurashi et al. (2000) (see Table 4b). Thus these comparisons are in qualitative agreement with the analyses based on the comparisons with AVHRR-derived optical depths.

The model-predicted reflected flux near 10°N appears to be low relative to the ERBE flux in all of the models, especially over the Pacific Ocean. This is a region where the modeled optical depths are also smaller than the

TABLE 4b. Comparison with satellite retrieval of Higurashi et al. (2000) and Nakajima and Higurashi (1998).

	CCMI–GRANTOUR		ULAQ		MPI–Dalhousie		GISS		ECHAM–GRANTOUR		GOCART		Mean of models	
Latitude	O.D.	Flux	O.D.	Flux	O.D.	Flux	O.D.	Flux	O.D.	Flux	O.D.	Flux	O.D.	Flux
−55.00	−0.01	−0.50	0.00	−0.13	0.04	3.81	−0.03	−3.17	−0.06	−6.75	0.10	10.70	0.01	0.54
−45.00	−0.01	−0.79	−0.03	−2.00	−0.05	−3.20	−0.07	−4.01	−0.06	−3.51	0.06	3.64	−0.03	−1.69
−35.00	−0.02	−1.35	−0.04	−2.02	−0.06	−3.63	−0.06	−3.27	−0.06	−2.81	0.02	1.29	−0.03	−1.96
−25.00	−0.04	−2.22	−0.03	−1.46	−0.07	−3.65	−0.07	−3.38	−0.06	−3.18	−0.01	−0.52	−0.04	−2.38
−15.00	−0.06	−3.40	−0.04	−2.30	−0.10	−4.97	−0.09	−4.51	−0.08	−4.00	−0.04	−2.12	−0.07	−3.50
−5.00	−0.05	−3.14	−0.07	−3.62	−0.09	−4.84	−0.09	−5.65	−0.06	−2.91	−0.05	−3.14	−0.07	−3.78
5.00	−0.06	−4.61	−0.08	−4.51	−0.10	−6.32	−0.08	−4.49	−0.04	−2.92	−0.06	−4.10	−0.07	−4.39
15.00	−0.06	−3.74	−0.01	−0.83	−0.11	−5.86	−0.05	−2.75	−0.05	−2.09	−0.03	−1.62	−0.05	−2.67
25.00	−0.03	−1.82	0.04	2.22	−0.04	−2.25	−0.04	−2.17	−0.04	−1.81	0.02	1.11	−0.01	−0.76
35.00	−0.02	−1.27	0.05	2.57	0.01	0.75	0.01	0.18	−0.04	−2.14	0.07	3.84	0.01	0.68
45.00	−0.03	−1.37	0.04	2.26	0.02	1.27	0.01	0.73	−0.06	−3.62	0.10	6.02	0.01	0.77
55.00	−0.02	−1.80	0.04	2.28	0.01	0.43	0.02	1.39	−0.06	−4.60	0.11	5.99	0.02	0.83
Global average	−0.04	−2.34	−0.02	−0.86	−0.06	−2.84	−0.05	−2.82	−0.06	−3.20	0.01	1.04	−0.04	−1.80

retrieved optical depths from all three retrievals. Sea salt, dust, sulfate, and organic aerosols all contribute to the optical depths in this region (see Fig. 4).

In all models the predicted reflected radiation is too small relative to ERBE in the region 10° to 30°S. This discrepancy also agrees with the analyses based on AVHRR-derived optical depths. Some of this discrepancy can be alleviated using the higher sea salt fluxes derived from the SSM/I analysis, especially in July, but the sensitivity test using these higher fluxes with the ECHAM–GRANTOUR model does not remove all of the discrepancy with the AVHRR-analyzed optical depth. The discrepancy might also be removed if higher emissions for biomass burning aerosols were assumed at these latitudes.

The shortwave radiative flux has a tendency to be overestimated by the models near 50°S relative to ERBE. As for the region north of 30°N, the comparison of annual average optical depth for most of these models is also larger than the satellite-retrieved optical depths according to Stowe et al. (1997); but as noted above, this is not necessarily the case when the models are compared to the retrievals by Mishchenko et al. (1999) and Higurashi et al. (2000).

To examine the relationship between the comparison of the models with ERBE-reflected flux and the comparison of the models with AVHRR-derived optical depth more quantitatively, we used the clear-sky aerosol forcing per unit optical depth from the ERBE analysis to scale the monthly average optical depth difference computed for the AVHRR analyses. These differences are summarized under the columns labled ''flux'' in Table 4 as well as in the last column of Table 5. In addition, Fig. 8 shows a plot of the difference between the 4-month average mean from the models and the 4-month average ERBE-reflected flux together with the infrared difference from the AVHRR analyses. As noted above, the character of the model difference with ERBE and the model difference with AVHRR is similar though details differ. For example, the reported flux difference from ERBE is higher at high latitudes than the reported flux difference from the AVHRR analyses. There is also a larger flux difference between the model mean and ERBE than between the model mean and AVHRR near the equator, though this feature is not present for every model. The 4-month average flux difference between the model mean and ERBE is 1.6 W m^{-2}, while that for the mean of the AVHRR analyses is -1.7 W m^{-2}.

6. Discussion and conclusions

As noted above, since clear scenes identified from both AVHRR and ERBE likely suffer from cloud contamination (Wielicki and Parker 1992; Mishchenko et al. 1999), the AVHRR-derived aerosol optical depths and ERBE clear-sky shortwave fluxes may be overestimated. More stringent cloud screening would likely reduce differences between the model and observations

TABLE 4c. Comparison with satellite retrieval of Stowe et al. (1997).

	CCMI–GRANTOUR		ULAQ		MPI–Dalhousie		GISS		ECHAM–GRANTOUR		GOCART		Mean of models	
Latitude	O.D.	Flux	O.D.	Flux	O.D.	Flux	O.D.	Flux	O.D.	Flux	O.D.	Flux	O.D.	Flux
−55.00	0.05	2.73	0.08	5.71	0.06	4.55	0.01	1.02	−0.02	−2.06	0.18	13.42	0.06	4.35
−45.00	0.02	1.17	0.00	0.09	−0.01	−0.64	−0.03	−1.99	−0.03	−1.65	0.09	5.90	0.01	0.45
−35.00	0.01	0.33	0.00	−0.43	−0.02	−1.81	−0.03	−1.87	−0.03	−1.39	0.06	2.66	−0.01	−0.42
−25.00	0.00	−0.19	0.01	0.53	−0.03	−1.86	−0.03	−1.61	−0.02	−1.40	0.04	1.10	−0.01	−0.58
−15.00	−0.02	−1.44	0.00	−0.41	−0.05	−3.22	−0.05	−3.00	−0.04	−2.29	0.01	−0.70	−0.03	−1.83
−5.00	−0.03	−2.18	−0.04	−2.60	−0.06	−3.94	−0.07	−5.06	−0.04	−2.19	−0.03	−2.43	−0.05	−2.99
5.00	−0.03	−4.24	−0.05	−4.04	−0.07	−6.11	−0.06	−3.94	−0.02	−3.18	−0.03	−3.59	−0.06	−4.09
15.00	−0.04	−2.40	−0.02	−0.09	−0.09	−4.75	−0.04	−1.63	−0.03	−1.40	−0.02	−0.39	−0.04	−1.67
25.00	−0.02	0.08	0.05	3.42	−0.04	−0.91	−0.02	−0.64	−0.02	−0.62	0.02	2.71	0.01	0.62
35.00	−0.01	−0.20	0.05	2.06	0.02	2.03	0.01	0.69	−0.02	−1.48	0.07	4.28	0.02	1.17
45.00	−0.02	−0.76	0.03	2.10	0.04	3.27	0.04	3.03	−0.04	−3.20	0.09	5.37	0.02	1.52
55.00	−0.02	−0.22	0.06	3.57	0.04	2.87	0.04	3.02	−0.06	−4.39	0.11	7.02	0.03	2.13
Global average	−0.01	−0.84	0.01	0.47	0.00	−1.40	−0.02	−1.35	−0.04	−2.04	0.06	2.19	−0.01	−0.47

in the region between 10° to 30°S, but may exagerrate differences at high latitudes. We conclude that there is a need for better cloud screening in satellite-based aerosol climatologies before any firm conclusions regarding the adequacy of model-calculated aerosol optical depth might be made. Much more reliable clear-sky fluxes are expected from the CERES instrument, which uses high-resolution imagers (i.e., visible infrared scanning radiometer and MODIS) for scene identification, thereby significantly reducing errors due to cloud contamination.

If we accept the satellite-derived optical depths and reflectivities as accurate, then for both north of 30°N and near 50°S, the comparison of modeled shortwave flux with ERBE suggests that the modeled optical depths are too high, while comparison with AVHRR suggests that the modeled optical depths are in the correct range (depending on the model). If the modeled optical depths are actually too high in the region north of 30°N, then estimates of forcing associated with industrial aerosols may be too high. But since sea salt aerosols also contribute in a significant manner to the optical depth in this region, the flux of sea salt or the extinction coefficient for sea salt may be overestimated. If the flux of sea salt or the extinction coefficient for sea salt is reduced this would also increase the correspondence between modeled and measured reflectivities near 50°S. However, smaller sea salt fluxes or extinction properties would increase the discrepancies between the models and satellite data in the region between 10° and 30°S.

Figures 6d–g displays the difference between the optical depth from the ECHAM–GRANTOUR model and the 4-yr averaged AVHRR aerosol optical depths from Mishchenko et al. (1999) with those derived from using the GOCART sea salt fluxes, doubled DMS fluxes, optical parameters for SO_4^{2-} derived from the assumption that the molar ratio of nitrate and ammonia to sulfate is 4, and optical parameters for biomass aerosols and other carbon aerosols derived from the biomass parameterization used in Penner et al. (1998). Even though this version of the ECHAM–GRANTOUR model produces optical depths that are similar to those from the models with a higher range of optical depths (Fig. 5), the comparison in Figs. 6d–g still shows significant differences from that of the AVHRR-analyzed optical depths. Arguably, this implies that if the model is still low relative to the observed optical depths and if this is true for each model, then the source of aerosols is too small.

Perhaps the best explanation of the differences between the models and the satellite measurements is that there is a missing non-sea salt open-ocean source that would increase optical depths in the region 10° to 30°S. To match a shortfall in optical depth in open-ocean regions requires higher optical depths than can be explained by increasing the DMS flux by a factor of two particularly in the months of April and October (see Figs. 5 and 6). Another possible explanation is that the source of aerosols from biomass burning is too low.

TABLE 5. Difference between model-predicted clear-sky shortwave radiative flux and ERBE satellite-measured clear-sky fluxes. Last column is the difference between the model mean flux and the infrared from the average of the three AVHRR analyses.

Latitude	CCMI–GRANTOUR	ULAQ	MPI–Dalhousie	GISS	ECHAM–GRANTOUR	GOCART	Mean of models	
							ERBE	AVHRR
−55.00	7.84	8.84	2.39	6.52	2.59	8.56	6.12	−1.58
−45.00	5.47	3.90	1.53	4.11	1.50	7.83	4.06	−2.13
−35.00	0.72	0.06	−2.17	−0.44	−1.90	3.22	−0.08	−1.69
−25.00	−2.22	−1.43	−4.68	−3.22	−3.88	−0.66	−2.68	−1.77
−15.00	−2.93	−2.38	−5.99	−4.57	−4.82	−2.30	−3.83	−2.67
−5.00	0.78	−1.31	−3.05	−1.42	−0.91	0.64	−0.88	−3.34
5.00	1.39	−0.97	−2.27	0.86	0.29	1.60	0.15	−3.88
15.00	0.23	1.59	−3.87	1.13	−1.82	1.60	−0.19	−2.02
25.00	1.92	6.82	−0.18	4.40	0.81	6.10	3.31	−0.47
35.00	5.43	9.22	3.46	9.43	1.78	9.61	6.49	0.14
45.00	3.54	9.04	4.38	9.92	1.75	12.05	6.78	0.71
55.00	3.99	6.30	3.10	8.79	1.66	12.31	6.02	0.07
Global average	1.76	2.74	−1.09	2.34	−0.52	4.33	1.59	−1.70

Indeed, the comparison of optical depths in Fig. 6 appears to suggest that the sources of biomass aerosols from Africa or Southeast Asia may need to be increased.

While this model-satellite data comparison has attempted to draw general conclusions regarding the adequacy of model-based estimates of aerosols based on this overall comparison of models and data, more definitive studies will require both improved estimates of sources and a better understanding of the relative accuracy of different model treatments of aerosol removal and transport. More accurate satellite analyses of aerosol optical depths are also needed.

Acknowledgments. The authors thank the NASA Aerosol Climatology Program for support. We also thank Brent Holben for sharing the AERONET program data and Stefan Kinne for a thorough review of the paper.

REFERENCES

Andres, R. J., and A. D. Kasgnoc, 1998: A time-averaged inventory of sub-aerial volcanic sulfur emissions. *J. Geophys. Res.,* **103D,** 25 251–25 261.

Atlas, R. M., R. N. Hoffman, S. C. Bloom, J. C. Jusem, and J. Ardizzone, 1996: A multiyear global surface wind velocity dataset using SSM/I wind observations, *Bull. Amer. Meteor. Soc.,* **77,** 869–882.

Barrie, L. A., and Coauthors, 2001: A comparison of large scale atmospheric sulphate aerosol models (COSAM): Overview and highlights. *Tellus,* in press.

Benkovitz, C. M., M. T. Scholtz, J. Pacyna, L. Tarrason, J. Dignon, E. C. Voldner, P. A. Spiro, J. A. Logan, and T. E. Graedel, 1996: Global gridded inventories of anthropogenic emissions of sulfur and nitrogen. *J. Geophys. Res.,* **101,** 29 239–29 253.

Carrico, C. M., M. J. Rood, and J. A. Ogren, 1998: Aerosol light scattering properties at Cape Grim Tasmania during the First Aerosol Characterization Experiment (ACE 1). *J. Geophys. Res.,* **103,** 16 565–16 574.

Chin, M., R. B. Rood, S.-J. Lin, J. F. Müller, and A. M. Thompson, 2000: Atmospheric sulfur cycle simulated in the global model GOCART: Model description and global properties. *J. Geophys. Res.,* **105,** 24 671–24 687.

Chuang, C. C., J. E. Penner, K. E. Taylor, A. S. Grossman, and J. J. Walton, 1997: An assessment of the radiative effects of anthropogenic sulfate. *J. Geophys. Res.,* **102,** 3761–3778.

Dentener, F. J., and P. J. Crutzen, 1994: A three-dimensional model of the global ammonia cycle. *J. Atmos. Chem.,* **19,** 331–369.

Deuzé, J. L., M. Herman, P. Goloub, D. Tanré, and A. Marchand, 1999: Characterization of aerosols over ocean from POLDER/ADEOS-1. *Geophys. Res. Lett.,* **26,** 1421–1424.

Feichter, J., E. Kjellstrom, H. Rodhe, F. Dentener, J. Lelieveld, and G.-J. Roelofs, 1996: Simulation of the tropospheric sulfur cycle in a global climate model. *Atmos. Environ.,* **30,** 1693–1707.

Ginoux, P., M. Chin, I. Tegen, J. Prospero, B. Holben, O. Dubovik, and S.-J. Lin, 2001: Sources and distributions of dust aerosols simulated with the GOCART model. *J. Geophys. Res.,* **106,** 20 225–20 273.

Gong, S. L., L. A. Barrie, and J.-P. Blanchet, 1997: Modeling sea-salt aerosols in the atmosphere. Part 1: Model development. *J. Geophys. Res.,* **102,** 3805–3818.

Guenther, A., and Coauthors, 1995: A global model of natural volatile organic compound emissions. *J. Geophys. Res.,* **100D,** 8873–8892.

Harrison, E. F., P. Minnis, B. R. Barkstrom, V. Ramanathan, R. D. Cess, and G. G. Gibson, 1990: Seasonal variation of cloud radiative forcing derived from the Earth Radiation Budget Experiment, *J. Geophys. Res.,* **95,** 18 687–18 703.

Haywood, J., V. Ramaswamy, and B. Soden, 1999: Tropospheric aerosol climate forcing in clear-sky satellite observations over the oceans. *Science,* **283,** 1299–1303.

Higurashi, A., T. Nakajima, B. N. Holben, A. Smirnov, R. Frouin, and B. Chatenet, 2000: A study of global aerosol optical climatology with two channel AVHRR remote sensing. *J. Climate,* **13,** 2011–2027.

Holben, B., and Coauthors, 2001: An emerging ground-based aerosol climatology: Aerosol optical depth from AERONET. *J. Geophys. Res.,* **106,** 12 067–12 097.

Jacob, D. J., and Coauthors, 1997: Evaluation and intercomparison of global atmospheric transport models using ^{222}Rn and other short-lived tracers. *J. Geophys. Res.,* **102,** 5953–5970.

Kahn, R. A., West, D. McDonald, B. Rheingans, and M. I. Mishchenko, 1997: Sensitivity of multiangle remote sensing observations to aerosol sphericity. *J. Geophys. Res.,* **102,** 16 861–16 870.

Kettle, A. J., and Coauthors, 1999: A global database of sea surface dimethylsulfide (DMS) measurements and a procedure to predict sea surface DMS as a function of latitude, longitude and month. *Global Biogeochem. Cycles,* **13,** 399–444.

Koch, D., D. Jacob, I. Tegen, D. Rind, and M. Chin, 1999: Tropospheric sulfur simulation and sulfate direct radiative forcing in

the Goddard Institute for Space Studies general circulation model. *J. Geophys. Res.*, **104,** 23 799–23 822.

Liousse, C., J. E. Penner, C. Chuang, J. J. Walton, H. Eddleman, and H. Cachier, 1996: A global three-dimensional model study of carbonaceous aerosols. *J. Geophys. Res.*, **101D,** 19 411–19 432.

Lohmann, U., J. Feichter, C. C. Chuang, and J. E. Penner, 1999: Prediction of the number of cloud droplets in the ECHAM GCM. *J. Geophys. Res.*, **104,** 9169–9198.

Mishchenko, M. K., I. V. Geogdzhayev, B. Cairns, W. B. Rossow, and A. A. Lacis, 1999: Aerosol retrievals over the ocean using channel 1 and 2 AVHRR data: A sensitivity analysis and preliminary results. *Appl. Opt.*, **38,** 7325–7341.

Nakajima, T., and A. Higurashi, 1998: A use of two-channel radiances for an aerosol characterization from space. *Geophys. Res. Lett.*, **25,** 3815–3818.

Nakicenovic, N., and Coauthors, 2000: *Emissions Scenarios. A Special Report of Working Group III of the Intergovernmental Panel on Climate Change.* Cambridge University Press, 599 pp.

Penner, J. E., H. Eddleman, and T. Novakov, 1993: Towards the development of a global inventory of black carbon emissions. *Atmos. Environ.*, **27A,** 1277–1295.

——, C. A. Atherton, and T. E. Graedel, 1994: Global emissions and models of photochemically active compounds. *Global Atmospheric–Biospheric Chemistry*, R. Prinn, Ed., Plenum Publishing, 223–248.

——, C. C. Chuang, and K. Grant, 1998: Climate forcing by carbonaceous and sulfate aerosols. *Climate Dyn.*, **14,** 839–851.

——, and Coauthors, 2001: Aerosols: Their direct and indirect effects. *Climatic Change 2001: The Scientific Basis*, J. T. Houghton et al., Eds., Cambridge University Press, 289–348.

Pitari, G., and E. Mancini, 2001: Climatic impact of future supersonic aircraft: Role of water vapour and ozone feedback on circulation. *Phys. Chem. Earth*, **2618,** 571–576.

——, ——, A. Bregman, H. L. Rogers, J. K. Sundet, V. Grewe, and O. Dessens, 2001: Sulphate particles from subsonic aviation: Impact on upper tropospheric and lower stratospheric ozone. *Phys. Chem. Earth*, **2618,** 563–569.

Quinn, P. K., and D. J. Coffman, 1998: Local closure during the First Aerosol Characterization Experiment (ACE 1): Aerosol mass concentration and scattering and backscattering coefficients. *J. Geophys. Res.*, **103,** 15 575–15 596.

Rasch, P. J., and Coauthors, 2000: A comparison of scavenging and deposition processes in global models: Results from the WCRP Cambridge Workshop of 1995, *Tellus*, **52B,** 1025–1056.

Stowe, L. L., A. M. Ignatov, and R. R. Singh, 1997: Development, validation, and potential enhancements to the second-generation operational aerosol product at the National Environmental Satellite, Data, and Information Service of the National Oceanic and Atmospheric Administration. *J. Geophys. Res.*, **102,** 16 923–16 934.

Tanré, D., L. A. Remer, Y. J. Kaufman, S. Mattoo, P. V. Hobbs, J. M. Livingston, P. B. Russell, and A. Smirnov, 1999: Retrieval of aerosol optical thickness and size distribution over ocean from the MODIS airborne simulator during TARFOX. *J. Geophys. Res.*, **104,** 2261–2278.

Tegen, I., and R. Miller, 1998: A general circulation model study of the inter-annual variability of soil dust aerosol. *J. Geophys. Res.*, **103D,** 25 975–25 995.

——, P. Hollrigl, M. Chin, I. Fung, D. Jacob, and J. Penner, 1997: Contribution of different aerosol species to the global aerosol extinction optical thickness: Estimates from model results. *J. Geophys. Res.*, **102,** 23 895–23 915.

Wielicki, B. A., and L. Parker, 1992: On the determination of cloud cover from satellite sensors: The effect of sensor spatial resolution. *J. Geophys. Res.*, **97,** 12 799–12 823.